An experimental study of the open end correction coefficient for side branches within an acoustic tube

Jianwu Dang
ATR Human Information Processing Research Laboratories, 2-2 Hikaridai, Seikacho Soraku-gun, Kyoto 619-02, Japan

Christine H. Shadle
Department of Electronics and Computer Science, University of Southampton, Southampton SO17 1BJ, United Kingdom

Yasuhito Kawanishi
Graduate School of Electronic Science and Engineering, Shizuoka University, Japan

Kiyoshi Honda
ATR Human Information Processing Research Laboratories, 2-2 Hikaridai, Seikacho Soraku-gun, Kyoto 619-02, Japan

Hisayoshi Suzuki
Department of Information Engineering, College of Science and Technology, Tohoku, Kunimi 6-45-16, Aoba-Ku, Sendai 982, Japan

The open end correction coefficient (OECC) of acoustic tubes has been widely investigated under a free-field condition. This study examines OECCs in confined regions, such as side branches within the vocal tract. To do this, a number of mechanical acoustic models are used to examine the effects of the angle of the branch axis and the proximity of the walls of the main tract to the open end of the branch. The OECC is estimated by matching both the peaks and troughs (i.e., spectral maxima and minima) of the computed and measured transfer functions for each model. The results indicate that the OECC of a side branch depends on L/D, where L is the cross dimension of the main tract at the branching point, and D is the branch diameter. For side branches connected to the main tract through a narrow neck, the OECC of each end of the neck is determined using the ratio of the radius of the neck to that of the adjacent section. Two empirical equations for evaluating the OECC within a tract are derived from the present study. Finally, the range of appropriate OECC values for estimating an accurate vocal tract transfer function is discussed, based on the results presented here and morphologic measurements reported previously. © *1998 Acoustical Society of America.* [S0001-4966(98)00408-1]

PACS numbers: 43.70.Bk, 43.70.Jt, 43.70.Aj [AL]

INTRODUCTION

It is well known that sound radiation takes place at any abrupt transition from a smaller cross-sectional area to a larger area in a compound acoustic system. The radiation makes the effective length of the section with the smaller area longer than its actual length. The ratio of the length increment to the radius of the smaller area is referred to as the open end correction coefficient (OECC). It has been proved that the OECC depends on the Helmholtz number kr (cf. Levine and Schwinger, 1948), where k is the wave number and r is the equivalent radius of the open end. In the field of speech production, the OECC is often used as a lumped coefficient in transmission line models for a low-frequency approximation.

Sound radiation at an abrupt area transition has been investigated under several conditions by a number of studies. Among them, Rayleigh (1945) gave theoretical descriptions in which the OECC is 0.785 for each side of an orifice in an infinitely thin plate, and is 0.824 when the plate becomes infinitely thick. Levine and Schwinger (1948) rigorously

solved the sound radiation for an unflanged circular pipe. They gave a theoretical value of the OECC, 0.6133, for a low-frequency approximation of the end correction. Nomura *et al.* (1960) examined the sound radiation at the open end of a flanged circular pipe numerically, and showed that the OECC for a flanged pipe is 0.8217 at low frequencies. Ando (1969) employed the same approach to analyze the sound radiation at the open end for various widths of the flange of the pipe, and the OECCs were consistent with the above solutions. Based on experimental data, Hall (1987) suggested the following empirical equation to describe the relation between the OECC and the width of the flange for a low-frequency approximation,

$$\alpha_1 = 0.821 - 0.13[(W/b) + 0.42]^{-0.54}, \qquad (1)$$

where b is the radius of the open end and W is the width of the flange. Peters *et al.* (1993) estimated OECCs under conditions in which the geometry at the open end of pipes was varied with and without a mean flow. The OECC obtained for a hornlike open end under the condition with no flow was approximately 0.46 (adjusting their value by taking the

OECC ratio in terms of the horn radius rather than the pipe radius), which is much lower than the previously suggested value of 0.6133. They showed that the OECC changed with geometries at the open end of pipes, larger for a sharp edge and smaller for a rounded one. In other words, the OECC in a compound acoustic system is related to the abruptness of the area transition between the adjacent sections. They also demonstrated that the OECC for large mean flow is low and independent of the flange thickness; for small mean flow the OECC becomes relatively constant, but the value of the constant depends on aspects of the geometry such as flange thickness, ranging between 0.6 and 0.8.

In contrast to free-field conditions, OECCs appropriate for confined regions have not been so extensively studied. Ingard (1953) examined the radiation of sound at the neck of a Helmholtz resonator, and suggested the following formula to evaluate the OECC for the interior end of the neck:

$$\alpha_2 = 0.48(A)^{0.5}[1/r - 1.25/R], \tag{2}$$

where A and r are the area and radius of the smaller-area section. R is the radius of the larger-area section, with r smaller than $0.4R$. El-Raheb and Wagner (1980) examined the effects of the sharp bends and branches of acoustic tubes for a given cross-sectional area and gave distributions of the sound pressure within the acoustic tubes. They showed that some different patterns of the transverse mode occurred for the rectangular pipes and the circular pipes. Since the dimensions of the vocal tract are much smaller than those of their tube models, such phenomena shown in their study would appear in a higher frequency region for a tube with dimensions similar to the vocal tract. However, most of the studies on speech production are more concerned with a low-frequency region which meets the assumption of plane-wave propagation.

In modeling the vocal tract, a number of side branches in the vocal tract such as the nasal tract, paranasal sinuses, and piriform fossa must be taken into account (see Fig. 1). The OECC is a significant factor in accounting for an abrupt area transition, large area ratios, and in most cases, short branch lengths. Partially due to a lack of experimental data for confined regions, however, the OECC values previously used in vocal tract models differ widely.

Fant proposed 0.8 as the OECC for a low-frequency approximation. He also recommended the use of Ingard's equation [Eq. (2)] to compensate for the radiation inductance of an abrupt area transition within the vocal tract such as the area between the teeth (Fant, 1970). Sundberg (1974) employed a value of 0.7 as the OECC to evaluate the acoustic characteristics of the piriform fossa. Dang and Honda (1996b) and Dang et al. (1996) estimated an OECC of 0.75 for the piriform fossa using MRI-based mechanical and numerical models. Koyama (1966), in evaluating the antiresonances of the paranasal sinuses, used an OECC value of 1.46 for the abrupt area transition at the two ends of the ostia, 0.73 for each end. On the other hand, Masuda (1992) reported that no end correction was necessary (i.e., the OECC equaled zero) for the ostia of the paranasal sinuses according to a comparison of his morphology-based computation with measured antiresonances.
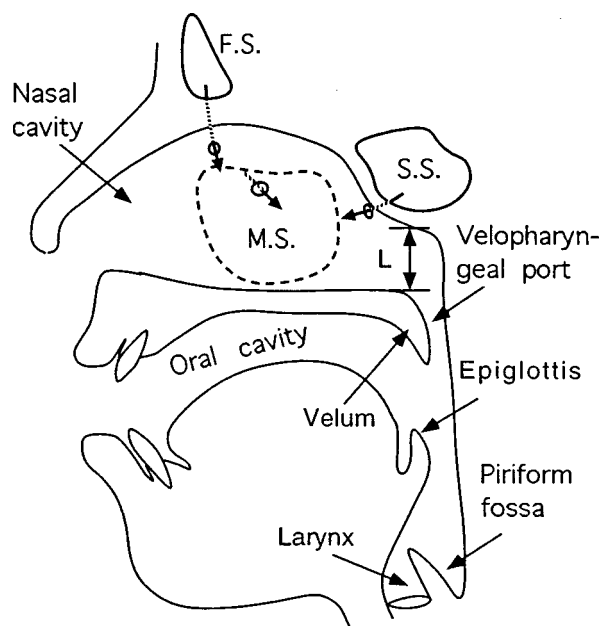

FIG. 1. A diagram of a sagittal view of the vocal tract showing the major side branches. L is the distance from the nasal floor to the ceiling of the nasopharynx. M.S., F.S., and S.S. are the maxillary, frontal, and sphenoidal sinuses.

According to previous studies (Hall, 1987; Peters et al., 1993), the geometry of the open end is a factor affecting the acoustic radiation. This factor is expected to be more dominant in the vocal tract because the geometries around the open end of the side branches are much more complex in the vocal tract than those discussed in the literature cited above. According to MRI-based morphological studies (see Dang et al., 1994; Dang and Honda, 1996c, 1997), the branches show various geometric shapes, and the dimensions of the main tract and the open end of the branches differ significantly from each other. Figure 1 shows a diagram of the major side branches within the vocal tract. At the bifurcation of the nasal and oral tracts, for example, the velopharyngeal port opens into the oral tract at the bend of the velum, and is directed almost opposite to the direction of sound propagation in the vocal tract. Contrarily, the direction of the opening of the piriform fossa is parallel to the direction of sound propagation, and the lateral walls of the fossa are continuous with the posterior and lateral walls of the pharynx. This geometry is expected to enhance the radiation reactance of the open end. The directions of the ostium openings of the paranasal sinuses to the nasal tract differ from one another, and the cross dimension of the main tract is relatively small in the vicinity of the open end. Radiation reactance at the open end of the branches is expected to be different for these different geometries.

In this study, a number of mechanical models with various branches were constructed to imitate the geometries of the side branches in the vocal tract. OECCs were estimated for the side branches within the mechanical models. The purpose of the present study was to provide experimental evidence to support the use of particular values of lumped-coefficient compensation for the radiation at the ends of side branches within the vocal tract model.
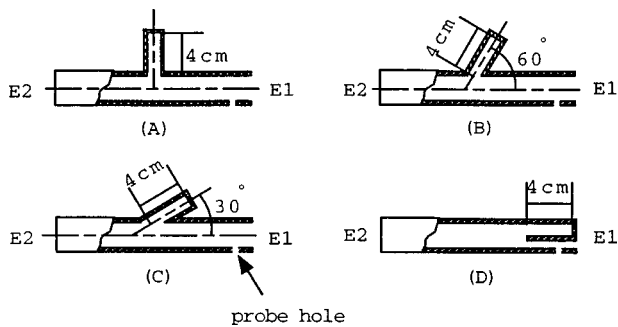
FIG. 2. Diagrams of mechanical models A through D, designed with different branch angles.

FIG. 3. A diagram of the experimental setup for measuring the transfer function of an acoustic tube.

I. EXPERIMENTAL PROCEDURE

The experimental procedures employed in this study were (1) design and construction of mechanical models with various side branches; (2) measurement and calculation of the transfer functions of the mechanical models; and (3) estimation of the optimal OECC for the side branches based on the computed and measured transfer functions.

A. Construction of the mechanical models

Acoustic experiments were designed to obtain a realistic OECC for vocal tract models. To this end, a number of mechanical models were constructed to imitate the geometries of the side branches in the vocal tract. The main tract was made from hard acrylic plates with a thickness of 0.3 cm. The cross-sectional shape of the main tract was designed to be square, and thus side branches in the tract had a plane opening end. Two types of side branches with a uniform area were employed: a tube with a circular cross section, and a tube with a rectangular cross section. The circular tube was attached about midway along the main tract on the outside of one of the walls. The rectangular tube was placed inside the main tract by partitioning one of the ends.

Figure 2 shows diagrams of four basic models. Models A, B, and C were 18.5 cm long and 2.6×2.6 cm in their inner cross section, while model D was 19.5 cm in length and 2.1×2.1 cm in its inner cross section. The branch in models A, B, and C was a circular tube with a length of 4 cm and a diameter of 1.7 cm, where the length was measured along the branch's central axis from the closed end to the open end. The branch in model D was 4 cm long and 2.1×1.0 cm in its cross-sectional size. The branch angles of the models were 90, 60, 30, and 0 degrees, respectively. These four models were used to examine the effects of different angles of the side branch axis to the main tract. To install the probe tube of a probe microphone for acoustic measurements, holes with a 0.12-cm diameter were drilled in the main tract wall about 1 cm back from either end.

Additionally, three more models, E, F, and G, were constructed for further examinations. Model E (diagramed in Fig. 6) was used for examining effects of the flange of the open end of the side branch, and of the proximity to the main tract wall. Model F (in Fig. 7) was designed to determine effects on the OECC of the branch diameter and the distance between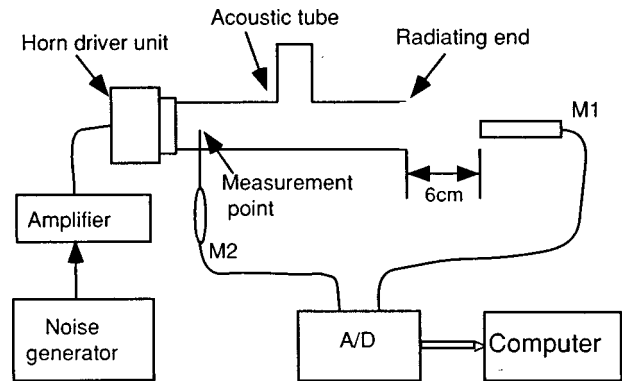 the open end and the opposite wall. Model G (in Fig. 10) was for estimating the OECC of a side branch with a narrow neck. Two identical holes, 1 cm apart, were drilled for the probe tube in the main tract wall near the input end for models E, F, and G.

B. Measurements

The pressure-to-pressure transfer function of the mechanical models was measured using a two-point pressure method, with which the acoustic properties of the side branch can be exactly described by measuring simultaneously the sound pressure in the main tract on the source side of the branch and the sound pressure from the radiating end of the main tract (Dang and Honda, 1996a). A diagram of the experimental setup used for measuring the two pressures is shown in Fig. 3. Microphone 1, B&K 4003, was placed 6 cm away from the radiating end to record the radiated sound. The probe tube of probe microphone 2, B&K 4128, was installed through the hole drilled in the main tract wall on the source side of the branch. A white-noise signal produced by an FG-143 function generator (NF Circuit Design Block Co.) was amplified and fed into an SG-505FRP horn driver unit (Goto Unit Co.) to excite the mechanical model. The join between the model and the neck of the horn driver unit was sealed with plasticine to prevent sound leakage. The outside sound pressure in the vicinity of the join was confirmed to be about 25 dB lower than that at the radiating end. This implies that sound leakage from the join can be considered to be negligible in this measurement. Sound recording was carried out at a sampling rate of 48 kHz in an anechoic room. A room temperature of 20 °C was maintained during the measurement, and therefore the sound velocity used in all calculations was 34 300 cm/s.

The two sound pressures were recorded simultaneously for 5 s for each measurement. Averaged power spectra of the sound pressures were computed using DFT with a 340-ms Hamming window shifting by 85 ms over the entire 5-s signal duration. The ratio of the power spectra of the radiated sound to the internal sound was taken to be the pressure-pressure transfer function of the segment from the internal measurement point to the radiating end.

The antiresonance of the side branch can be identified in the measured transfer function. However, the antiresonance may not appear clearly in the transfer function if it is located

1077   J. Acoust. Soc. Am., Vol. 104, No. 2, Pt. 1, August 1998

Dang et al.: Open end correction coefficient   1077

near a resonance. Our previous studies demonstrated that adjusting the location of the internal measurement point can move the resonances in the transfer function without affecting the antiresonance frequencies of the side branch (Dang and Honda, 1996a, c). In essence, the resonances correspond to the resonances of the tube open at both ends, with one end corresponding to the open end and the other to the location of the internal measurement point. For this reason, two probe holes as described previously were designed for models E, F, and G to change the internal measurement point. Thus antiresonances that may be distorted or obscured by nearby resonances for one internal measurement point can be revealed through this procedure.

Strictly speaking, a factor for the transfer from the main tract end to M1, which is in the near field, should be included. As a check, transfer functions were measured for different positions of M1, varying the distance from the open end to M1 from 3.5 to 30 cm. It was found that there were some changes in the amplitude of the baseline of the measured spectra and in the slope of the envelope, but not in the resonance or antiresonance frequencies. Since in this study we are more interested in these frequencies, this factor was omitted.

C. Estimation of OECC

Since the interaction between the resonances and antiresonances in an acoustic system tends to obscure or distort each other, frequencies of maxima and minima in a measured transfer function are usually different from the true resonances and antiresonances to some extent. We therefore refer to maxima and minima in the measured transfer functions as peaks and troughs, respectively, and compare the measured and computed transfer functions in order to establish the frequencies of the true resonances and antiresonances. A transmission-line model was employed to compute the transfer function for the comparison. If both the troughs and peaks in the computed transfer function are matched well to those in the measured one, it is reasonable to assume that the acoustic properties of the computational model are identical to those of the mechanical model.

The transmission-line models had an identical area function to that of the measured tube segment, from M2 to the radiating end, with an adjustable OECC for the branch. The bifurcation point of the branch and main tract in the computational model was at the intersection of the branch's central axis and the open end for models A, B, C, F, and G, and at the edge of the open end of the branch for models D and E. The equivalent radius used for the square openings was approximated by a circular radius of $r = \sqrt{A/\pi}$, where A is the area of the opening. The radiation impedance of the main tract of the computational models was approximated by a cascaded connection of resistance and inductance (Caussé et al., 1984). Losses due to viscosity and heat conduction were implemented in the computation (Flanagan, 1972), while losses due to wall vibrations were ignored for these rigid-walled mechanical models. The validity of the acoustic parameters above was confirmed using a uniform straight tube.
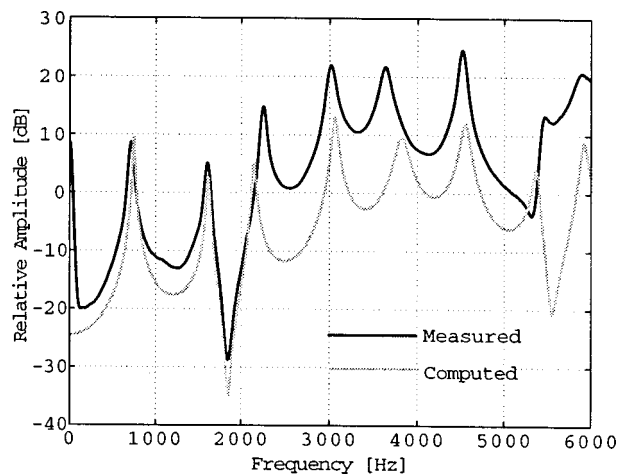

FIG. 4. A typical comparison of measured and computed transfer functions for a tract with a side branch; this case is model D.

In this estimation, the OECC for the branch was adjusted to match the computed troughs and peaks to the measured ones. The optimal OECC value was defined that satisfied the condition that the differences in both the peak and trough frequencies should be less than 3% for frequencies below 3 kHz. The OECC values found in this way will henceforth be referred to as *matched OECC values*, to distinguish them from OECC values derived from empirical formulas. Figure 4 shows an example of the comparisons between the measured and computed transfer functions for model D. In this example, the computation and the measurement are consistent within 3% below 3.5 kHz for the frequencies of the peaks and troughs, and within 5% above. The computed and measured transfer functions demonstrate almost identical spectral shapes at lower frequencies. These two spectra show an increasing disparity at higher frequencies. This is probably caused by the accumulated effects and the assumption of plane-wave propagation in the simulation, where the assumption is not always correct for higher frequencies. For this reason, the above comparison for the troughs was limited to the first trough of the branch, though the second trough was typically visible in the higher frequency region.

Figure 4 shows that as frequency increases, the amplitude difference between the spectra increases. This difference is mainly caused by the different tilts of the two spectra. The tilt is more pronounced for the measured spectrum because microphone 2, B&K 4128, has a decreasing response with increasing frequency (see the instruction manual of B&K 4128), while microphone 1, B&K 4003, has a flat response over a wide frequency region. Since there was no significant effect on the frequencies of the peaks and troughs either with or without calibration, noncalibrated data are used in obtaining the measured transfer function.

II. RESULTS

The results of the experiment are shown for the effects of (1) the angle of the branch to the main tract, (2) the flange of the open end of the branch and the surrounding wall of the
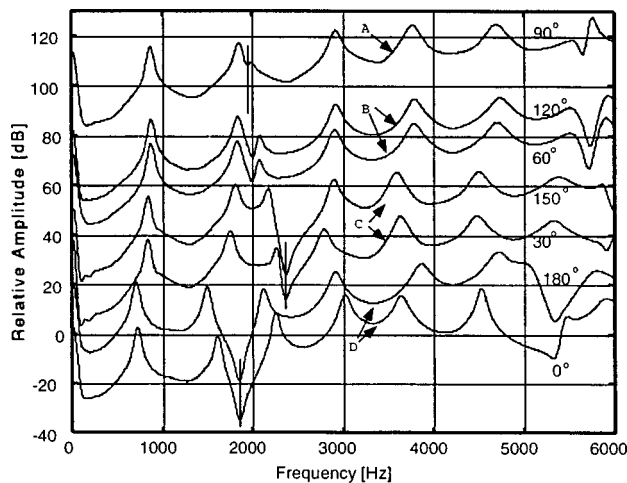
FIG. 5. Transfer functions measured for the mechanical models shown in Fig. 2 with the model label and branch angle for each curve. Successive curves are offset by 20 dB.

TABLE I. Trough frequencies measured from the transfer functions shown in Fig. 5, and matched OECCs (BA: branch angle).

Model	BA (Deg)	Troughs (Hz)	OECC
A	90	1940	0.48
D	0	1848	0.78
	180	1842	0.80
B	60	1991	⋯
	120	1997	⋯
C	30	2361	⋯
	150	2361	⋯

main tract, (3) the dimensions of the branch and the main tract at the bifurcation, and (4) a narrow neck within a side branch.

A. Effects of the angle of the side branch axis

Four mechanical models were used experimentally to determine effects of the angle of the side branch axis on the OECC. The mechanical models are shown in Fig. 2. The branch angle is defined as the angle between the central axis of the branch and that of the main tract, using angles in the range of 0–180 degrees. In models A through D, the branch angles are, respectively, 90, 60, 30, and 0 degrees when using E1 as the input end. Treating E2 as the input end, the corresponding branch angles for the same models are 90, 120, 150, and 180 degrees.

The measurements were carried out on the models twice, feeding sound from E1 and then E2. Thus, seven transfer functions were obtained from the models for the angles of 90, 60, and 120, 30 and 150, and 0 and 180 degrees. The measured transfer functions are shown in Fig. 5, given in pairs except for model A. Effects of the angles, if any, can be easily found from each pair for the same model, because the geometries surrounding the branches were exactly the same. The troughs occur at approximately the same frequency for each pair of transfer functions, but their amplitudes are slightly lower (the troughs are deeper) for the obtuse than for the acute angles, and the spectra surrounding the troughs show slightly different shapes. The frequency of the first trough is listed in Table I for each case. The trough frequencies show significant differences for varying branch angles across the four models. As could be predicted theoretically, there is no significant difference in the trough frequencies for the same model regardless of whether its branch angle is obtuse or acute. The consistency of the measurement with the theoretical prediction confirms the accuracy of our experimental procedure.

The OECCs of the branches in the models were also estimated using the method described in Sec. I C. For models B and C, however, the open end of the branch is not simply

defined in the computational model since the opening plane of the branch is not parallel to the wavefront for the plane-wave assumption (see El-Raheb and Wagner, 1980). Therefore it is not possible to obtain the OECCs for models B and C using the present method. For this reason, this estimation was limited to models A and D. Matched OECCs are shown in the fourth column of Table I for branch angles of 0, 90, and 180 degrees. The OECCs obtained for 0 and 180 degrees are not significantly different. Contrarily, the OECC for the branch angle of 90 degrees does differ significantly. The value of 0.48 for the 90 degrees case is much smaller than that proposed in previous studies (Rayleigh, 1945; Hall, 1987).

Since the branch angle is not a major factor affecting the OECC, it is suspected that the geometric shapes surrounding the open ends of the branches caused the difference. In model D, but not model A, the branch shares walls with the main tract. This structure may enhance the radiation reactance of the open end. Another difference is that the dimension of the main tract into which the branch opened is larger in model D than that in model A. To clarify the relations between the OECC and these aspects of the geometry, we conducted the following experiments.

B. Effects of the flange of the open end and the main tract wall

A mechanical model with a branch angle of 0 degree (model E, shown in Fig. 6) was used to examine the effects of the flange of the open end of the side branch and the main tract wall. The main tract was 10 cm long, with a cross section of 2.1×2.1 cm. The branch was 4.0 cm in length,
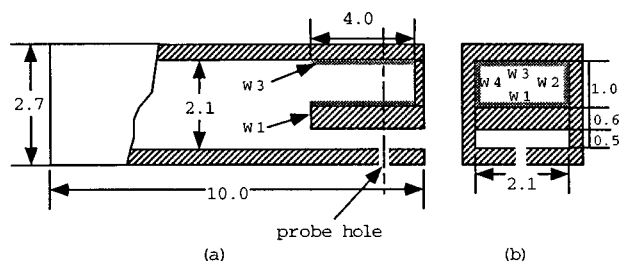

FIG. 6. Model E for examining effects of the flange of the open end of the side branch and the main tract wall. (a) Axial-sectional view; (b) cross-sectional view at the location of the probe hole. The layers added on the original walls are shown by W1, W2, W3, and W4. All dimensions are in cm.

TABLE II. Condition 1: thickening wall W1 in model E. Branch dimensions, measured troughs, and matched OECCs are listed.

W1 thickness (cm)	Branch end area (cm^2)	Troughs (Hz)	OECC
0.6	2.10	1845	0.79
0.7	1.89	1845	0.83
0.8	1.68	1848	0.87
0.9	1.47	1863	0.87
1.0	1.26	1877	0.88
1.1	1.05	1895	0.88

TABLE IV. Condition 3: thickening walls W2 and W4 in model E. Branch dimensions, measured troughs, and matched OECCs are listed.

W2, W4 thickness[a] (cm)	Branch end area (cm^2)	Troughs (Hz)	OECC
0.0	2.10	1842	0.80
0.1	1.90	1851	0.81
0.2	1.70	1863	0.81
0.3	1.50	1877	0.81
0.4	1.30	1883	0.85

[a]The value shown is the thickness of the insert on each side.

and 2.1×1.0 cm in its cross section. Measurements of the transfer function of this model were made under three conditions:

Condition 1: Vinyl chloride plates with an area of 4.0×2.1 cm and a thickness of 0.1 cm were glued on the partition wall, W1, one by one. This manipulation was done in order to explore effects of the flange width of the open end in a confined region by thickening W1 while retaining the proximity to the main tract walls. The measurement was repeated while the thickness of W1 increased from 0.6 to 1.1 cm in 0.1-cm steps.[1]

Condition 2: Plates identical to those used in condition 1 were glued on the main tract wall (W3, referred to as the back wall) to decrease the effects of the proximity by moving the open end of the branch away from the main tract wall. The measurement was repeated while increasing the thickness of the inserts from 0 to 0.5 cm at 0.1-cm intervals.

Condition 3: Two identical plates with an area of 4.0×1.0 cm and a thickness of 0.1 cm were glued on two opposite sides of the branch simultaneously (W2 and W4) to decrease the proximity to the lateral walls of the main tract. The measurements were carried out while the thickness of each side insert increased from 0 to 0.4 cm with intervals of 0.1 cm.

The measured trough frequencies and matched OECCs are shown in Table II for condition 1. The matched OECCs increase as wall W1 is thickened. This tendency is consistent with those obtained by Ando (1969) and by Hall (1987). Thickening W1 from 0.6 to 1.1 cm increases the OECC from 0.79 to 0.88, a total change of 0.09, or 11%. This implies that the effect of the flange of an open end in a confined space is the same as that in a free field.

The matched OECCs for condition 2 are shown in Table III. At first, the OECC decreases as flange W3 increases from 0.0 to 0.1 cm. It then remains nearly constant as the thickness of W3 increases from 0.1 to 0.4 cm. Changing W3 in

TABLE III. Condition 2: thickening wall W3 in model E. Branch dimensions, measured troughs, and matched OECCs are listed.

W3 thickness (cm)	Branch end area (cm^2)	Troughs (Hz)	OECC
0.0	2.10	1845	0.79
0.1	1.89	1868	0.76
0.2	1.68	1880	0.76
0.3	1.47	1894	0.76
0.4	1.26	1909	0.76
0.5	1.05	1921	0.77

this way can apparently be considered to involve two main components: increase of the flange thickness and decrease of the proximity to the main tract wall. According to the result for condition 1, thickening the flange increases the OECC. However, no such tendency was seen under condition 2 even though the thickness of flange W3 was increased by the same amount. It can be concluded that decreasing the proximity to the main wall has the opposite effect, i.e., it tends to decrease the OECC. In other words, when the branch wall continues directly into the main tract, the open end effect of the branch is greatly enhanced.

Under condition 3, the matched OECCs increase slightly, unlike in condition 2. This tendency shown in Table IV implies that the effect of decreasing the proximity to the lateral walls is smaller than that of thickening the flanges. The difference between conditions 2 and 3 indicates that the lateral walls had a smaller effect than the back wall, although the length of the boundary between the lateral walls and the branch was about the same as that between the back wall and the branch. If one simply imagines the effective open end of the branch to extend diagonally from W1 to the back wall (so that the length of the back wall effectively ''belonging'' to the branch is longer than the partition wall W1), this phenomenon is easily understood. With this conjecture, the magnitude of the effect of the lateral walls on the OECC is approximately half that of the back wall for the same boundary length.

Summarizing the above results, thickening W1 increases the thickness of the flange and shortens the length of the boundary between the lateral walls and the branch, but it does not change the situation between the back wall and the branch. Therefore it can be concluded that thickening the flange enhances the OECC. Thickening W3 under condition 2 showed a different behavior from that produced by thickening W1 under condition 1. One of the causes may be that an extra abrupt area transition was added to the branch with W3 under condition 2. However, since adding an abrupt area transition should enhance the end radiation and this tendency was not seen in the result, the extra abrupt area transition is not the major cause of the difference. Considering the common results under conditions 2 and 3, the major cause seems to be due to the decrease of the proximity to the main tract wall; it results in acoustically reducing the effective length of the branch. In other words, the proximity to the main tract wall contributes to increasing the effective length of the branch.
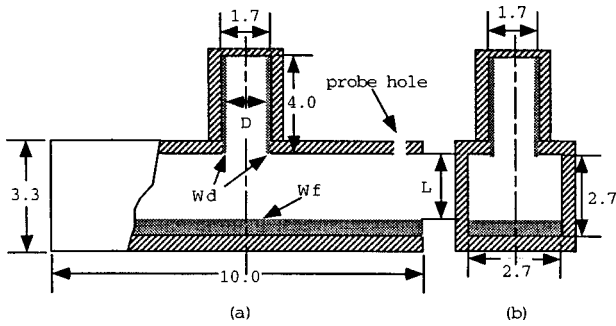
FIG. 7. Model F for investigating the relationship between the OECC and the dimensions of the main tract and the branch at the bifurcation. (a) Axial-sectional shape; (b) Cross-sectional shape. All dimensions are in cm.

C. Effects of the dimensions at the bifurcation

Figure 7 shows a diagram of model F which was used to examine the effects of the dimensions of the main tract and the branch at the bifurcation. The main tract was 10 cm long and 2.7×2.7 cm in its inner cross section. The branch, a circular uniform tube, was 4 cm in length and 1.7 cm in diameter. Effects of the dimensions of the branch and the main tract in the vicinity of the bifurcation were examined by varying two dimensions systematically: the inner diameter of the branch, D, was decreased by increasing the thickness of W_d; and the distance L across the main tract was decreased by increasing the thickness of W_f. D was decreased from 1.7 to 0.7 cm in 0.2-cm steps by gluing layers of stainless steel foil, 0.1 cm thick, on the inner wall of the branch. For each value of D, L was varied from 2.7 to 0.6 cm in 0.3-cm steps by gluing an acrylic plate with an area of 10×2.7 cm and a thickness of 0.3 cm on wall W_f.

Figure 8 shows the matched OECCs for all of the combinations of L and D. The figure demonstrates that OECCs increase with L for a given branch diameter D. For a given L, the OECCs increase as D decreases. The curves of the OECCs move in parallel with D.

The results show that the OECC is approximately proportional to distance L and inversely proportional to the diameter of the open end of the branch. To arrive at a general
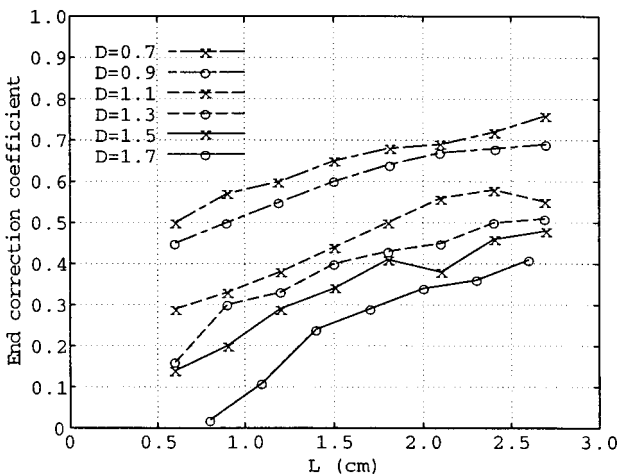

FIG. 8. Matched OECCs for various combinations of L and D for model F, shown in Fig. 7.
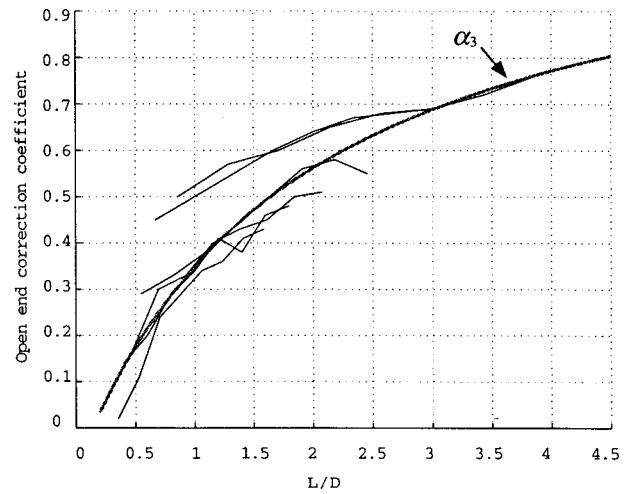

FIG. 9. Matched OECCs of Fig. 8 plotted against dimensionless parameter L/D. See Fig. 7 for the definitions of L and D. The line marked α_3 is the least-squares fit to all of the curves shown.

relationship of the OECCs to the parameters, the data were replotted against a dimensionless parameter L/D. As shown in Fig. 9, the six curves of the matched OECCs collapse approximately onto a curve that is a function of L/D. A least-square method was used to calculate the best-fitting curve. This curve, which we call the *estimated OECC*, is plotted in Fig. 9, and is given by the following empirical formula:

$$\alpha_3 = \frac{1.27\xi}{\xi + 1.92} - 0.086, \quad 0.2 < \xi = \frac{L}{D} < 4.5, \qquad (3)$$

where α_3 is the estimated OECC for model F, D is the inner diameter of the open end of the branch, and L is the distance from the open end to the opposite wall of the main tract. The mean-square error was 0.048 between the measurements and the prediction by this formula. Considering the conditions of the measurement and application, the formula is appropriate to be used in a range of $\xi = L/D$ between 0.2 to 4.5, where α_3 ranges from 0.03 to 0.80.

D. End corrections for a branch with a narrow neck

In the vocal tract, there are a number of branches with a narrow neck, such as the paranasal sinuses in the nasal cavity. A neck has two ends: one opening into the main tract, referred to as the tract end; and the other one opening into the cavity, referred to as the cavity end. Both ends require an end correction for the abrupt area transitions. The tract end of the branch neck has a similar geometry to that discussed for model F. For this end, therefore, the correction coefficient can be evaluated using Eq. (3). In this section we arrive at an estimate for the OECC for the cavity end of the branch neck.

A mechanical model shown in Fig. 10, referred to as model G, was used in this examination. This model consisted of a main tract with a square cross-sectional shape of 2.7 $\times 2.7$ cm, and a circular branch with a narrow neck. The cavity of the circular branch was 3.8 cm in length and 1.7 cm in inner diameter. The neck length l_N was chosen to be 0.3 cm which is approximately equal to the ostium length of the
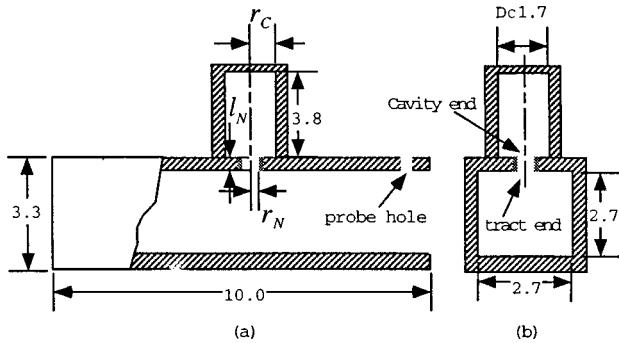
FIG. 10. Model G, used for estimating the OECC for the cavity end of the branch neck as a function of neck diameter $D_N = 2r_N$. l_N is the length of the neck. All dimensions are in cm.

maxillary sinus, the biggest side branch in the nasal tract. Diameter, D_N, of the neck was varied as described below.

Transfer functions of model G were measured while varying the diameter of the neck (D_N) from 0.17 to 1.0 cm in 12 steps. In the measured transfer functions, for $D_N > 0.5$ cm, a second trough appeared at a higher frequency. This implies that the branch can no longer be modeled as a simple Helmholtz resonator. Accordingly, this branch was treated as a tract with two cascaded sections in this estimation of the OECC.

As mentioned above, the OECC of the tract end was evaluated using Eq. (3). For $L/D > 4.5$, the OECC was reasonably assumed to be 0.80. As shown in Fig. 11 (broken line), this region occurs in model G for $r_N/r_C < 0.35$, where r_N=radius of the branch neck and r_C=radius of the branch cavity.

In order to estimate the OECC for the cavity end of the branch neck, the computed transfer function was matched to the measured one while the OECC was adjusted. The optimal OECCs were obtained when the measured and computed transfer functions were consistent with one another within

1% for the first trough, and within 2% for the first two peaks. Figure 11 shows the matched OECCs for the cavity end (plotted using an asterisk), which decrease monotonically from 0.712 to 0.069 as the ratio of radii increases. To derive a general empirical formula, an expression similar to that used by Ingard (1953) was adopted to describe the experimental data. The parameters in the expression were derived based on the measurements with a constraint that the OECC be equal to 0.821 when $\xi = 0$ (Nomura *et al.*, 1960). By minimizing the mean least square of errors between measurement and prediction, we arrive at the expression:

$$\alpha_4 = 0.821(1 - 1.69\xi), \quad \xi < 0.6, \tag{4}$$

where $\xi = r_N/r_C$. Values of α_4 (solid line) are plotted in Fig. 11 as ξ is varied, which predicts the matched OECCs with a mean-square error of 0.053. This result indicates that the end radiation is negligible when the ratio ξ is larger than 0.6 even if an abrupt area transition exists.

III. DISCUSSION

In this section, we summarize the effects of the geometries on the OECC of a side branch, and compare the predictions of our formulas with previous results. The range of OECCs for the side branches within the vocal tract is also discussed based on the present results and morphologic measurements reported previously.

A. Summary of the measurements

A number of mechanical models were designed with various side branch shapes to imitate the geometries of the side branches within the vocal tract. With these models, acoustic effects of the geometries on the antiresonances and the OECCs of the branches were examined. The angle of the branches with respect to the main tract was varied; this did not show any significant effects on the antiresonance frequencies, nor on the matched OECCs in the cases where they could be estimated. Two cases, i.e., the branches parallel to and perpendicular to the main tract, however, showed different behaviors.

The parallel-branch case (model E) showed an interaction of the effects on the OECC of the branch flange and the proximity to the wall of the main tract. General speaking, the OECC is higher for a branch within a main tract than the same ''branch'' in a free field. This effect is heightened as the branch open end approaches the main wall of the tract.

The perpendicular-branch case (model F) showed an interaction of the effects on the OECC of the diameter (D) of the branch's open end and the distance (L) from the end to the far wall of the main tract. This effect was strong enough to allow us to collapse all of the matched OECCs onto one curve using the dimensionless parameter L/D. These collapsed curves can be predicted well using an empirical formula [Eq. (3)]. As shown previously, this formula is derived for a given width of the main tube. What are the possible effects on the formula if the width of the main tube varied? Basically, increasing the width of the main tube has two simultaneous actions: thickening the flange and reducing the proximity of the lateral walls to the branch open end, and
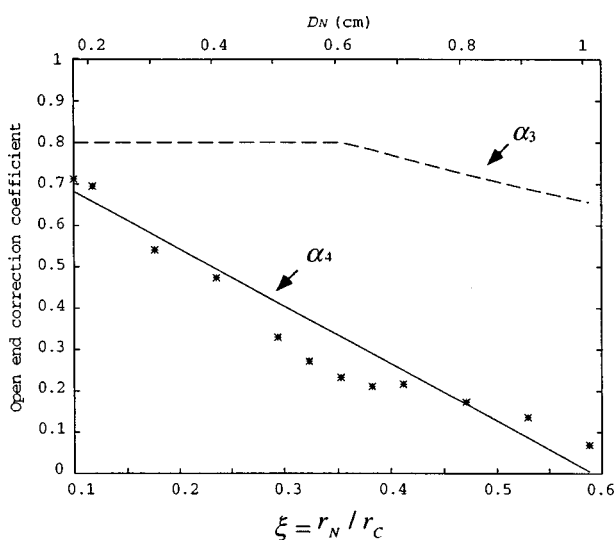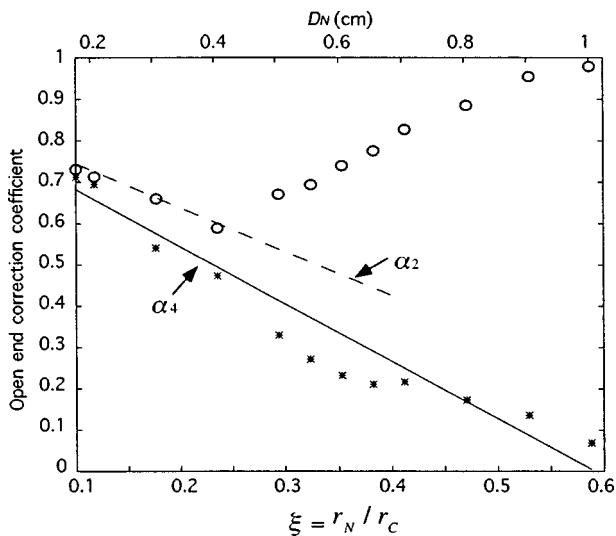

FIG. 11. Predictions and measurements for model G, Fig. 10. With the OECCs of the tract end of the neck evaluated using Eq. (3) (broken line), the OECC of the cavity end of the neck was matched using a cascaded-tube treatment (''*''), and an empirical approximation [Eq. (4)] to that is shown (solid line). r_N and r_C are defined in Fig. 10. D_N is the diameter of the neck.

FIG. 12. OECCs for the cavity end of the neck of model G: matched using a Helmholtz resonator treatment (○), using a cascaded-tube treatment (∗), and predicted using our formula Eq. (4) (solid line) and Ingard's formula Eq. (2) (dashed line). r_N, r_C, and l_N are defined in Fig. 10. In Ingard's notation, $\xi = r/R$.

vice versa. According to the results obtained in Sec. II B, the OECC increases when widening the flange, and decreases when reducing the proximity of the wall. These two effects occur simultaneously when varying the main tube width, and counteract one another to some extent. This interaction was proved in the results under conditions 2 and 3 of model E, which have a smaller range of variation than that of condition 1, when only the flange is changed. When the width of the main tube becomes wide enough, the effects of both the flange and the lateral wall on the OECC become constant. Accordingly, it can be concluded that the relationship of L and D in this formula is not affected significantly by varying the width of the main tube.

This study also derived an empirical expression [Eq. (4)] from the measurements of model G for predicting the OECC of a side branch with a neck, where the branch was treated as a cascaded tube. The expression has different parameters from Ingard's [Eq. (2)], which was derived for the Helmholtz resonator. To compare these two formulas, the data obtained in Sec. II D were reprocessed by treating the branch as a Helmholtz resonator. Figure 12 shows the matched OECCs obtained from the resonator-treatment (indicated by an open circle), and the OECCs predicted from Ingard's formula (broken line), and our Eq. (4) (solid line). Unlike the cascaded-tube treatment (shown by an asterisk), the OECCs from the resonator-treatment at first decrease and then, for $D_N > 0.5$, increase. This is also the point at which higher-frequency troughs were observed in the transfer functions. Therefore the following discussion is limited to the region where the neck diameter D_N is smaller than 0.5. In this limited region, the matched OECCs (open circle) are consistent with those estimated using Ingard's formula [Eq. (2)] within 2%, and within 15% for our formula [Eq. (4)]. This shows that Ingard's formula gives more accurate estimates than our formula when the branch can be treated as a Helmholtz resonator. However, one can see in Fig. 12 that our formula can offer a good prediction for the more general case. Therefore we conclude that our formula is better in general for the end correction at an abrupt area transition of the vocal tract.

B. The OECC for side branches within the vocal tract

The morphologies of side branches in the vocal tract were investigated by the authors using magnetic resonance imaging (MRI) (Dang et al., 1994; Dang and Honda, 1996c, 1997). In this section we combine vocal tract data with the OECC estimates derived above to arrive at a range of OECCs appropriate for the branches within the vocal tract.

The nasal tract is the largest branch occurring in the vocal tract. When the velum is lowered, an abrupt area transition of the velopharyngeal port occurs on both the oral side and the nasal side as shown in Fig. 1. On the oral side, the geometry is most similar to model E, where the side branch is considered equivalent to the entire nasal tract. Thus the posterior wall of the pharynx, which runs continuously from the "main tract" into the "side branch," would be predicted to enhance the radiation from the open end of the nasal tract. According to our measurements from model E, an OECC greater than 0.8 is required to compensate for the open end radiation.

On the nasal side, the geometry surrounding the velopharyngeal port shows features of both model F and model E, i.e., there is a limited distance (corresponding to L) between the open end and a wall of the nasal tract, and this wall is also continuous with the main tract (see Fig. 1). According to Peters et al. (1993), the OECC for the open end of the nasal side is smaller than that estimated by the models, because of its horn-shaped edge. In contrast, the posterior wall of the nasopharynx enhances the radiation reaction. Since these two effects are expected to counteract each other to some extent, the OECC of the open end on the nasal side can be approximated using model F. According to our observations (Dang et al., 1994), the distance L from the open end to the ceiling of the nasopharynx was approximately 1.5 cm for nasal sounds, averaging over four subjects. During nasal consonants, the area of the velopharyngeal port is typically about 1.7 cm^2 on the nasal side, and thus the equivalent diameter (D) is about 1.47 cm. An OECC of about 0.35 is predicted using Eq. (3) for an average value. In the transition from a nasal consonant to a nasalized vowel, the area of the velopharyngeal port decreases and the edge of the port gets sharper. In this case, the OECC is expected to increase. For example, when the area of the port is reduced to 0.5 cm^2, the OECC increases to 0.54. The end radiation at both sides of the velopharyngeal port can lower the first nasal formant to some extent. This may explain the fact that the first nasal formant in speech sounds is lower than that in morphology-based synthetic sounds. The discrepancy may be partly due to the OECCs for the branches, in addition to the other acoustic effects of the paranasal sinuses reported previously (Dang et al., 1994; Dang and Honda, 1996c).

In the case of the paranasal sinuses, morphological data of the ostia are available only for the maxillary sinuses (Dang et al., 1994; Dang and Honda, 1996c). The geometry of the nasal side of the ostia is similar to model F. According to our measurements (Dang et al., 1994), the diameter of the

ostia was about 0.38 cm, and the distance from the ostium opening to the opposite wall was about 0.3 cm. The OECC of the ostia on the tract side was predicted to be about 0.28 using Eq. (3). However, the OECC for the cavity side should be about 0.8 since the narrow neck opens to a relatively large cavity.

The geometry of the piriform fossa resembles model E, because the posterior and lateral walls of the pharynx enhance the radiation of the fossa end. However, model E is too simple to account for the geometrical complexity near the open end of the piriform fossa. A detailed discussion is available elsewhere (Dang and Honda, 1996c, 1997; Dang *et al.*, 1996).

Besides the side branches, there are three major abrupt area transitions along the vocal tract: the outlet of the larynx, the region around the epiglottis, and the area between the teeth (the lips are not discussed here because they open to a free field). The abrupt area transition at the epiglottis is obvious for front vowels such as /i/ and /u/, but not evident for back vowels such as /a/. Since front vowels have a relatively large pharynx, the effect of the abrupt area transition in this region is small. In the boundary of the laryngeal and pharyngeal tubes, the ratio of the radii of the larynx's outlet to the pharynx varies with vowels, and ranges from 0.28 to 0.60 for English vowels (Story and Titze, 1996). The OECC based on formula (4) ranges from 0.0 to 0.43, which hardly contributes to the acoustic characteristics of the vocal tract. An end correction of the opening at the teeth can be of more importance than that of the others, since the constriction formed by the teeth is usually short. Empirical formula (4) can be used to estimate the OECC in this case.

Applications of these empirical formulas from the present study have been discussed with regard to the vocal tract. Since details of the vocal tract shape are not completely known and the mean flow within the vocal tract changes during a dynamic articulation, some additional conditions possibly remain to be discovered.

ACKNOWLEDGMENTS

[1] The Helmholtz number kr is also a factor affecting the OECC, where k is the wave number and r is the equivalent radius of the open end of the branch. In all of the cases discussed here, trough frequencies ranged from 1842 to 1921 Hz and the equivalent radii were 0.58–0.82 cm (see Tables II–IV). The Helmholtz number kr ranged from 0.20 to 0.29 for the changes in the geometry. According to previous studies (Levine and Schwinger, 1948; Ando, 1969; Peters *et al.*, 1993), the OECC can be considered to be approximately independent of the Helmholtz number for this range of 0.20–0.29.

Ando, Y. (**1969**). ''On the sound radiation from semi-infinite circular pipe of the certain wall thickness,'' Acustica **22**, 219–225.

Caussé, R., Kergomard, J., and Lurton, X. (**1984**). ''Input impedance of brass musical instruments—Comparison between experiment and numerical model,'' J. Acoust. Soc. Am. **75**, 241–254.

Dang, J., and Honda, K. (**1996a**). ''A new method for measuring antiresonance details of the vocal tract transmission characteristics—An experimental study of acoustic tubes,'' J. Acoust. Soc. Jpn. (E) **17**, 93–96.

Dang, J., and Honda, K. (**1996b**). ''Acoustical modeling of the vocal tract based on morphological reality: Incorporation of the paranasal sinuses and the piriform fossa,'' Proceedings of the 1st ESCA Tutorial and Research Workshop on Speech Production Modeling: from Control Strategies to Acoustics & 4th Speech Production Seminar: Models and Data, Autrans, France, pp. 49–52.

Dang, J., and Honda, K. (**1996c**). ''Acoustic characteristics of the human paranasal sinuses derived from transmission characteristic measurement and morphological observation,'' J. Acoust. Soc. Am. **100**, 3374–3383.

Dang, J., and Honda, K. (**1997**). ''Acoustic characteristics of the piriform fossa in models and humans,'' J. Acoust. Soc. Am. **101**, 456–465.

Dang, J., Honda, K., and Suzuki, H. (**1994**). ''Morphological and acoustical analysis of the nasal and the paranasal cavities,'' J. Acoust. Soc. Am. **96**, 2088–2100.

Dang, J., Kawanishi, Y., and Shadle, C. (**1996**). ''Estimation of correction coefficient and location of the radiating end of the piriform fossa,'' Proceedings of the Spring Meeting of Acoust. Soc. Jpn. (in Japanese), pp. 287 and 288.

El-Raheb, M., and Wagner, P. (**1980**). ''Acoustic propagation in rigid sharp bends and branches,'' J. Acoust. Soc. Am. **67**, 1914–1923.

Fant, G. (**1970**). *Acoustic Theory of Speech Production* (Mouton, The Hague), 2nd ed.

Flanagan, J. L. (**1972**). *Speech Analysis Synthesis and Perception* (Springer-Verlag, New York), 2nd ed.

Hall, D. E. (**1987**). *Basic Acoustics* (Wiley, New York).

Ingard, U. (**1953**). ''On the theory and design of acoustic resonators,'' J. Acoust. Soc. Am. **25**, 1037–1061.

Koyama, T. (**1966**). ''Experimental study on the resonance of paranasal sinus,'' J. Otolaryngol. Japan **69**, 1177–1191 (in Japanese).

Levine, H., and Schwinger, J. (**1948**). ''On the radiation of the sound from an unflanged circular pipe,'' Phys. Rev. **73**, 383–406.

Masuda, S. (**1992**). ''Role of the maxillary sinus as a resonant cavity,'' J. Otolaryngol. Japan **95**, 71–80 (in Japanese).

Nomura, Y., Yamamura, I., and Inawashiro, S. (**1960**). ''On the acoustic radiation from a flanged circular pipe,'' J. Phys. Soc. Jpn. **15**, 510–517.

Peters, M., Hirschberg, A., Reijnen, A., and Wijnands, A. (**1993**). ''Damping and reflection coefficient measurements for an open pipe at low Mach and low Helmholtz numbers,'' J. Fluid Mech. **256**, 499–534.

Rayleigh, B. (**1945**). *Theory of Sound* (Dover, New York).

Story, B., and Titze, I. (**1996**). ''Vocal tract area function from magnetic resonance imaging,'' J. Acoust. Soc. Am. **100**, 535–554.

Sundberg, J. (**1974**). ''Articulatory interpretation of the singing formants,'' J. Acoust. Soc. Am. **55**, 838–844.